

Muscle contraction and the elasticity-mediated crosstalk effectNadiv Dharan¹ and Oded Farago^{1,2}¹*Department of Biomedical Engineering, Ben Gurion University of the Negev, Be'er Sheva 84105, Israel*²*Ilse Katz Institute for Nanoscale Science and Technology, Ben Gurion University of the Negev, Be'er Sheva 84105, Israel*

(Received 25 October 2012; revised manuscript received 15 March 2013; published 23 May 2013)

Cooperative action of molecular motors is essential for many cellular processes. One possible regulator of motor coordination is the elasticity-mediated crosstalk (EMC) coupling between myosin II motors whose origin is the tensile stress that they collectively generate in actin filaments. Here, we use a statistical mechanical analysis to investigate the influence of the EMC effect on the sarcomere—the basic contractile unit of skeletal muscles. We demonstrate that the EMC effect leads to an increase in the attachment probability of motors located near the end of the sarcomere while simultaneously decreasing the attachment probability of the motors in the central part. Such a polarized attachment probability would impair the motors' ability to cooperate efficiently. Interestingly, this undesired phenomenon becomes significant only when the system size exceeds that of the sarcomere in skeletal muscles, which provides an explanation for the remarkable lack of sarcomere variability in vertebrates. Another phenomenon that we investigate is the recently observed increase in the duty ratio of the motors with the tension in muscle. We reveal that the celebrated Hill's equation for muscle contraction is very closely related to this observation.

DOI: [10.1103/PhysRevE.87.052714](https://doi.org/10.1103/PhysRevE.87.052714)

PACS number(s): 87.19.Ff, 87.16.A–, 87.16.Ka, 87.16.Nn

I. INTRODUCTION

Skeletal striated muscles are tissues that contract in order to produce the movement of the body. The fundamental contractile unit of the muscle is the *sarcomere*, which is composed of two types of filaments, actin and myosin, in an arrangement that allows them to slide past each other [1]. Upon nervous stimulation, Ca^{2+} ions flow into the muscle cell and expose binding sites located on the actin filament [2]. The myosin thick filament consists of myosin II motor proteins with a lever arm structure that bind to the binding sites on the actin thin filament and, via ATP hydrolysis, change its conformation, resulting in a “power stroke” that propels the myosin filament on top of the actin filament [3]. Comparison of skeletal muscle cells in different vertebrates reveals that the lengths of their sarcomeres are almost identical. The length of the thick filament is usually found to be close to $1.6\ \mu\text{m}$, while the length of the thin filament is typically in the $0.95\text{--}1.25\ \mu\text{m}$ range [4]. This fact is striking considering the different tasks that different muscles perform in different species. Here, we argue that this remarkable feature of muscles is closely related to the ability of the myosin II motors to work in cooperation, which may be jeopardized by the elasticity-mediated crosstalk (EMC) effect arising from the compliance of the actin filament [5]. During muscle contraction, the application of opposite forces (the motor forces versus the external load) on the actin filaments causes large force fluctuations. This leads to an increase in the elastic energy stored in the filaments that can be lowered if the duty ratios of the myosin II motors are changed. Our analysis shows that, in contracting muscles, the EMC effect causes the attachment probability of motors to become nonuniform (spatially dependent). This feature negatively affects muscle performance since it hampers the ability of the motors to cooperate efficiently. Interestingly, this undesired phenomenon becomes significant only when the system size exceeds that of the sarcomere, which provides a plausible explanation for the similarity of the sarcomeres in muscle cells across vertebrates.

Our current understanding of the mechanics of muscle contraction is very much influenced by two classical works. The first one is Hill's work [6], in which the muscle was represented through a combination of elastic, contractile, and resistive (viscous) elements. Hill postulated that in overcoming the viscous resistance, the contracting muscle does work and produces heat. Through a general notion of energy balance and some empirical relations between the rate of heat production during muscle contraction and the contraction velocity, Hill derived his famous equation,

$$(P + a)(v + b) = (P_0 + a)b, \quad (1)$$

where P is the load opposing the contraction, v is the contraction velocity, P_0 is the isometric load (i.e., the load for $v = 0$), and a and b are constants. Although generally considered as a phenomenological force-velocity relationship rather than a thermomechanical expression, Hill's equation has drawn much attention because of its simplicity and the agreement it shows with experimental measurements [7].

The second seminal work is Huxley's crossbridge theory from 1957, which provides a molecular-level interpretation for muscle contraction [8]. Within the model, the myosin motor heads interact with specific binding sites along the actin filament to form elastic crossbridges. When a motor is attached to a binding site, the crossbridge stretches and force is applied on the actin filament, resulting in the relative movement of the actin (thin) and myosin (thick) filaments past each other. The attachment and detachment of motor heads to and from the actin filament are governed by “on” and “off” rate functions that regulate the fraction of crossbridges (i.e., attached motors), and which depend on the stretching energy of the crossbridges. The “on” and “off” rates were chosen by Huxley to obtain a good fit with Hill's experimental data for the force-velocity relationship [Eq. (1)].

Huxley's work, together with the development of improved methods for experimental determination of the sarcomere's microstructure [9], as well as new biochemical measurements

of ATP activity [10], have provided a fruitful field for further investigations. In 1971, a widely accepted four-state scheme for the mechanochemical cycle of myosin II was introduced by Lymn and Taylor [11]. More recently, Duke [12], and later others [13–18], came up with models that integrated the Lymn-Taylor scheme into the crossbridge model. Duke’s model (like Huxley’s) treats the motor heads as elastic elements with strain-dependent on and off rates. The model assumes that the viscous friction forces can be neglected in the equation of motion of the contracting muscle. The latter assumption remains controversial, and several alternative models incorporating viscous effects have also been proposed for the contractile process [19,20]. Both classes of models have been successful in producing Hill’s force-velocity relationship.

Another major success of the theoretical models is their ability to show that the fraction of working (force-producing) motors, r , increases with the load P . This feature has been recently observed by Lombardi and co-workers [21], who showed, by using x-ray scattering and mechanical measurements on the tibialis anterior muscles of frogs, that r increases from roughly $r = 0.05$ for $P = 0$ to $r = 0.3$ for the maximal isometric load. Related patterns of collective behavior also emerge in models for motor protein motility assays [22,23]. Specifically, several ratchet models have shown that when two groups of antagonistic motors are engaged in a “tug-of-war” competition, their detachment rates may be considerably varied [24–26]. Another setup, closely related to muscle contractility, is a single class of motors that work against the force produced by an optical trap [27]. One of the factors that significantly alters the detachment rates is the EMC, whose effect on muscle contractility is studied here using a simple spring-bead model.

II. HILL’S EQUATION

Before presenting our model and its results, we first wish to examine more closely the experimental results of Ref. [21]. To that end, it is useful to define the dimensionless variables $0 \leq x \equiv P/P_0 \leq 1$ and $0 \leq y \equiv v/v_{\max} \leq 1$, where v_{\max} is the maximum contraction velocity at $P = 0$. When expressed in terms of these variables, Hill’s equation (1) takes the dimensionless form

$$y = \frac{1-x}{1+cx}, \quad (2)$$

where c is a constant. Notice that Eq. (2) satisfies both the relation that $y = 1$ for $x = 0$ (load-free contraction) and $y = 0$ for $x = 1$ (isometric contraction). The other important notion in relation to muscle contraction is the observed [see Fig. 3(D) in Ref. [21]] increase in r with P , which is well approximated by the linear relationship

$$r = r_0 + (r_1 - r_0)x, \quad (3)$$

where r_0 and r_1 denote the attachment probability for $x = 0$ and 1, respectively. To match the experimental data, we set $r_0 = 0.05$ and $r_1 \simeq 0.3$. Since the sarcomere contracts at a constant velocity, then Newton’s first law of motion implies that the forces generated by the motors are balanced by the external load P and the friction forces in the system. The latter originate from two sources: the surrounding medium and the

crossbridges. The balance of forces reads

$$r(f_m - \lambda_m v) = \lambda v + \frac{P}{N}. \quad (4)$$

The expression in parentheses on the left-hand side of Eq. (4) can be identified as the force per motor,

$$f_0(v) = f_m - \lambda_m v. \quad (5)$$

It includes a positive “active force,” f_m , and a negative “motor-friction force” characterized by the motor friction coefficient λ_m [28]. This linear force-velocity relationship is consistent with the experimental results shown in Fig. 4(B) of Ref. [21]. On the right-hand side of Eq. (4) we have the counter external load, P/N , and the friction force caused by the surrounding medium, λv ($\lambda \neq \lambda_m$), both normalized per motor.

It is important to emphasize that Eq. (3) is empirical, and we do not intend to discuss its physical basis. Here, we simply want to demonstrate that Hill’s dimensionless equation can be derived from Eqs. (3) and (4) without any further assumptions. Explicitly, upon substitution of Eq. (3) in Eq. (4) and rearrangement of the resulting equation, one arrives to the following expression for the contraction velocity:

$$v = \frac{f_m r_0 (1-x)}{\lambda + \lambda_m [r_0 + (r_1 - r_0)x]}. \quad (6)$$

Also, for $P = 0$, Eq. (4) takes the form

$$\frac{f_m r_0}{v_{\max}} = \lambda + \lambda_m r_0. \quad (7)$$

Dividing Eq. (6) by v_{\max} and using Eq. (7) as well as the relation $P/N = x P_0/N = x f_m r_1$, one arrives at Eq. (2) with

$$c = \frac{\lambda_m (r_1 - r_0)}{\lambda + \lambda_m r_0}. \quad (8)$$

We further note that for $y = 1$ ($v = v_{\max}$), the following expression can be derived for f_0 if Eq. (7) is used in Eq. (5):

$$f_0|_{y=1} = f_m \frac{\lambda}{\lambda + r_0 \lambda_m}. \quad (9)$$

The experimental data [21] give $f_m = 6$ pN, $f_0|_{y=1} = 4$ pN, and $r_0 = 0.05$, which, upon substitution in Eq. (9), yields $\lambda_m = 10\lambda$. When this last result, together with the values for r_0 and r_1 , are used in Eq. (8), one arrives at $c = 5/3$, which is within the range $1.2 < c < 4$ where the constant c is typically found for skeletal muscles [29]. Notice that in order to match the experimental data, we included viscous terms in our derivation, which (as noted above) is a matter of controversy. Nevertheless, it is important to recognize that Eq. (8) has a well-defined limit when both λ and λ_m vanish, provided that λ/λ_m is finite.

III. MODEL

We now proceed to discuss the relevance of the EMC effect to skeletal muscle contraction. Figure 1(a) shows a schematic of the sarcomere structure, consisting of an array of parallel actin thin filaments surrounded by thick filaments of myosin motors. Adjacent sarcomeres are connected end-to-end to form *myofibrils*. The ends of the actin filaments are anchored at the Z-line, which transmits the external load to the actin filaments. Our model of the sarcomere is depicted in Fig. 1(b). The

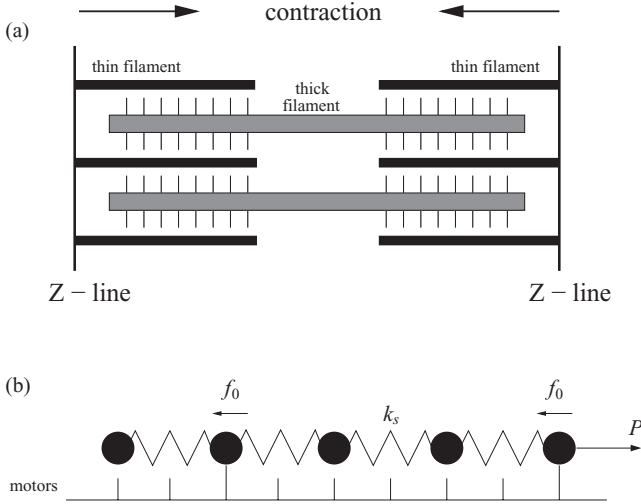


FIG. 1. (a) Schematics of the sarcomere, consisting of an array of parallel actin thin filaments surrounded by thick filaments of myosin motors. Adjacent sarcomeres are connected end-to-end at the *Z-line*. (b) In our model, the actin filament is represented as a chain of nodes, connected by identical springs with spring constant k_s . Each node is either connected to a single myosin II motor, in which case it experiences a force of magnitude f_0 , or disconnected, in which case it experiences no force. The motor forces are countered by the external force P which acts at the end of the chain.

elastic actin filament is modeled as a chain of N monomers connected by $N - 1$ elastic springs with spring constant k_s . We assume that a motor exerts a force of magnitude f_0 on the actin filament in the attached state, and no force in the detached state. The other model parameter is the attachment probability of the motors, r . As discussed above, both f_0 and r vary with v . Our model neglects spatial (motor-to-motor) and temporal variations of r and f_0 at a given v , so these two quantities represent the typical attachment probability and motor force, respectively. As we will demonstrate below, it is the EMC effect that leads to spatial variations in the *effective* (mean) attachment probability of the motors, which we will denote by $\langle r \rangle$ (to be distinguished from the uniform “bare” attachment probability r).

The motor forces work against the opposite external force which is applied on the N th last monomer. The tug-of-war competition between the motor forces and the external force stretches the actin filament. Denoting by E^{el} the elastic energy of the filament, the statistical weight of a configuration with n connected motors is given by $w = r^n (1 - r)^{N-n} \exp(-E^{\text{el}}/k_B T)$, where $k_B T$ is the thermal energy. We treat the elastic energy as an equilibrium degree of freedom (of a system which is inherently out-of-equilibrium) because the mechanical response of the filament to the attachment or detachment of motors is extremely rapid and occurs on time scales which are far shorter than the typical attachment time of the motors. The elastic energy E^{el} is calculated as follows [30]. We denote by f_i the force applied on the i th monomer, where $f_i = 0$ or $f_i = f_0$ for $i = 1, \dots, (N - 1)$, and $f_i = -P$ or $f_i = -P + f_0$ for $i = N$. The total elastic energy is the sum of spring energies, $E^{\text{el}} = \sum_{i=1}^{N-1} F_i^2/2k_s$, where F_i is the force applied on the i th spring. The forces F_i are calculated as

follows: We first calculate the mean force $\bar{f} = (\sum_{i=1}^N f_i)/N$ and define the excess forces acting on the nodes: $f_i^* = f_i - \bar{f}$. The force on the i th spring is then obtained by summing the excess forces applied on all the monomers located on one side of the spring: $F_i = -\sum_{l=1}^i f_l^* = \sum_{l=i+1}^N f_l^*$.

The model is studied by using Monte Carlo simulations with trial moves that attempt to change the state (connected or disconnected) of a randomly chosen motor. For each move attempt, the elastic energy E^{el} of the chain is recalculated, and the move is accepted or rejected according to the conventional Metropolis criterion with the statistical weights given by w .

IV. RESULTS

In half a sarcomere, each thick filament has about 150 motor heads [2]. To simulate muscles operating under conditions of optimal force generation, we assume that there is a full overlap between the thick and thin filaments [1], and we consider a chain with $N = 150/2 = 75$ monomers. (The division by 2 is due to the 1:2 ratio between thin and thick filaments.) We also simulate larger systems of $N = 150$ and 300 nodes and fix the model parameters to $r = 0.05$, $f_0 = f_m = 6$ pN, and $k_s \simeq 4.5$ N/m (see the discussion on how these values were set in [30]). Our simulation results for the mean attachment probability, $\langle r(i) \rangle$, as a function of i ($1 \leq i \leq N$), the position of the monomer along the chain, are depicted in Fig. 2 for $N = 75$ (a), $N = 150$ (b), and $N = 300$ (c). The simulations reveal that due to the EMC effect, the attachment probability becomes a monotonically increasing function of i . The origin of this feature is the fact that the springs are not equally stretched, as can be inferred from the above derivation of the elastic energy. Generally speaking, attachment of a motor to a certain node i leads to a reduction in the energy of the springs with $j < i$. For each N , there is a single node ($i = i^*$) where the attachment probability, $\langle r(i^*) \rangle$, is independent of P and takes a value which is very close to the bare attachment probability r . The difference between the attachment probabilities at both ends of the chain (i.e., for $i = 1$ and $i = N$) increases with both N and P . For $N = 75$, the variation in $\langle r(i) \rangle$ is quite small, becoming meaningful only at near-stall forces $P/(f_0 N) \simeq 0.05$. In contrast, for $N = 150$, the variations in $\langle r(i) \rangle$ are significant and may be as large as $\langle r(N) \rangle / \langle r(1) \rangle \gtrsim 4$. The mean attachment probability, $\langle r \rangle \equiv [\sum_{i=1}^N \langle r(i) \rangle] / N$, is plotted in Fig. 2(d) as a function of P . For both $N = 75$ and 150 and for all values of P , we find that $\langle r \rangle \simeq r$, which shows that the decrease in $\langle r(i) \rangle$ for $i < i^*$ is almost offset by the increase in $\langle r(i) \rangle$ for $i > i^*$. This is not the case for $N = 300$, where $\langle r \rangle$ exhibits a steady increase with P . The increase in $\langle r \rangle$ is due to the fact that at large forces (notice that the applied loads are proportional to N), the attachment probability $\langle r(i) \rangle$ becomes a rapidly increasing function of i . The implication of the rise in $\langle r \rangle$ is that the stall force *per motor* increases to $\simeq 0.1 f_0$ (from $\simeq 0.05 f_0$ for $N = 75$ and 150).

The above results seem to indicate that for $N > 75$, the variations in $\langle r(i) \rangle$ may be sufficient to disrupt muscle performance. However, one needs to recall that the simulation results depicted in Fig. 2 correspond to fixed values of r and f_0 , while

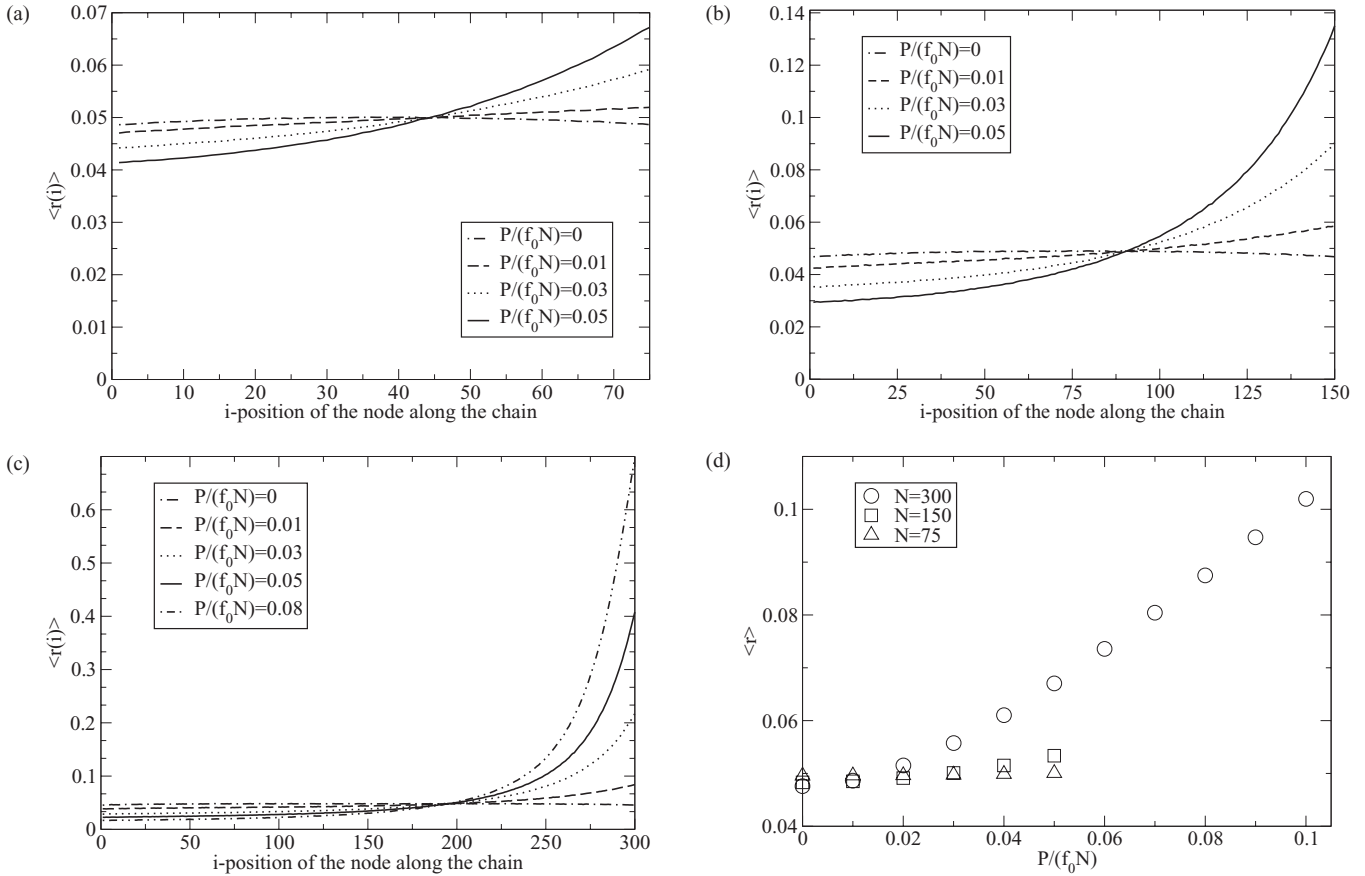


FIG. 2. The attachment probability $\langle r(i) \rangle$ to the i th chain node, calculated for chains consisting of (a) $N = 75$, (b) $N = 150$, and (c) $N = 300$ nodes. For each N , the attachment probability is plotted for various values of the load P . (d) The effective attachment probability $\langle r \rangle$ as a function of the dimensionless load per motor $P/(f_0 N)$ for $N = 75$ (triangles), $N = 150$ (squares), and $N = 300$ (circles).

in reality the values of these quantities vary with the shortening velocity v . Therefore, we also performed simulations where for each value of P , the appropriate value of v is chosen and, accordingly, the values of r and f_0 are set. This has been done by using Eqs. (2), (3), and (5), as outlined in the Appendix. Our results for the sarcomere simulations are summarized in Fig. 3, which shows the position-dependent attachment probability, $\langle r(i) \rangle$, calculated for a chain of size $N = 75$ and for different loads. Similarly to the results plotted in Fig. 2(a), the results here indicate that $\langle r(i) \rangle$ remains fairly uniform for $1 \leq i \leq N = 75$. This observation is consistent with the motor mechanochemistry, where at high and medium velocities v the detachment of motors occurs after the completion of the power stroke. In the mechanochemical picture, the detachment rate can be estimated by $\tau_{\text{det}}^{-1} \sim v/\delta$, where δ is the size of the power stroke ($\delta \sim 6 \text{ nm}$ [21]), and this rate must be the same for all the motors. Highly polarized detachment probability hampers the motors' ability to cooperate and, thus, constitutes an undesired effect. Notice that Fig. 3(a) features a small increase in the attachment rate near the Z-line (for $y > 0.2$). This, in fact, represents a “positive” effect, as it enables the muscle to sustain a larger load. We stress that the discussion here is relevant only for high and medium velocities where the motors attach, execute the power stroke, and then unbind. At very low velocities ($y \simeq 0$) close to the isometric load ($x \simeq 1$), the motors may detach and reattach multiple times before the

power stroke is completed [31]. The number of attachments per power stroke need not be the same for all the motors and, therefore, variations in the attachment probabilities (which are indeed observed in Fig. 3 at small values of y) can be tolerated in this limit without negative consequences for muscle contractility.

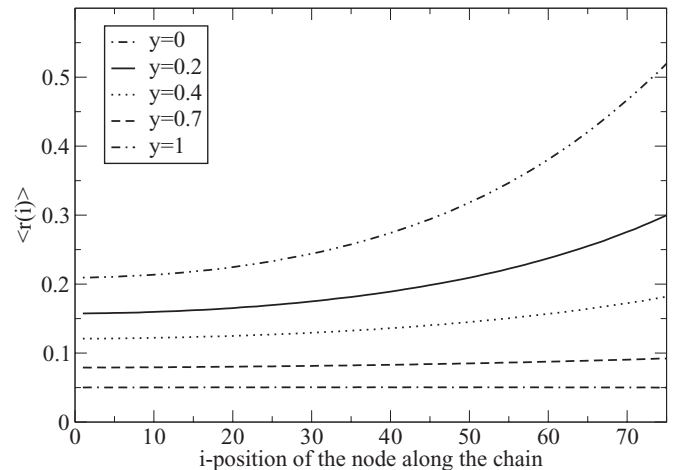


FIG. 3. The attachment probability $\langle r(i) \rangle$ to the i th chain node, calculated for different values of the rescaled velocity y .

V. SUMMARY

We found that the EMC effect leads to an increase in the attachment probability (duty ratio) of motors located near the Z-line while simultaneously decreasing the attachment probability of the motors in the central part of the sarcomere (M-line). The resulting variations in the attachment probabilities of the motors pose a serious problem for muscle performance because the detachment rate of the motors is primarily determined by the size of the power stroke and the muscle shortening velocity and, therefore, should be fairly uniform. We used a simple bead-spring model to demonstrate that this undesired effect can be almost neglected for half-sarcomeres consisting of fewer than approximately $2N = 150$ motors, which is precisely the “universal” size of half a sarcomere. Recent advances in single molecule techniques [32] have paved the way for testing our theoretical predictions concerning the polarization of the attachment probability. Specifically, optical tweezers provide the means to apply pico-Newton forces against the gliding motion of the thin filament, while the duty ratio may be directly measured using high-resolution atomic force microscopy (AFM).

ACKNOWLEDGMENTS

We thank Sefi Givli for numerous insightful discussions.

APPENDIX: DETAILS OF THE SARCOMERE SIMULATIONS

In the simulations depicted in Fig. 3, the values of x (rescaled load), y (rescaled velocity), f_0 (motor force), and r (duty ratio) are different for each curve. Their values are set by using Eqs. (2), (3), and (5), with system parameters that are chosen to match the experimental results of Ref. [21]. For a given value of y , the value of x is determined from Hill’s

equation (2),

$$y = \frac{1-x}{1+(5/3)x}, \quad (\text{A1})$$

while the value of f_0 is set according to Eq. (5),

$$f_0 = 6 \left(1 - \frac{y}{3}\right) \text{ (pN)}. \quad (\text{A2})$$

The determination of r is slightly more complicated. The complication arises due to the fact that the bare attachment probability r appearing in Eqs. (3) and (4) should be replaced with the effective attachment probability, $\langle r \rangle$, which is the experimentally measured quantity and which is not known *a priori*. Therefore, for each value of y we simulated different values of r and, using linear interpolation, we determined the value of r that yields the desired $\langle r \rangle$. As can be inferred from Fig. 3, the difference between r and $\langle r \rangle$ is quite small for high and medium velocities.

Another important comment is the following: If the excess forces used in the calculation of the elastic energy are expressed in units of the motor force f_0 , $\tilde{F}_i \equiv F_i/f_0$, then the Boltzmann weight of a configuration with n connected motors can be written as

$$w = r^n (1-r)^{N-n} \exp\left(-\beta^* \sum_{i=1}^{N-1} \tilde{F}_i^2\right), \quad (\text{A3})$$

where $\beta^* = f_0^2/2k_s k_B T$. In the simulations presented in Fig. 2, the motor force is taken as $f_0 = f_m = 6$ pN, while the spring constant $k_s = 4.5$ N/m. This means that at a physiological temperature of $T = 310$ K, $\beta^* \simeq 10^{-3}$, which is the value of β^* used in the simulations depicted in Fig. 2. In Fig. 3, we use the above Eq. (A2) to evaluate f_0 . This means that for each curve in Fig. 3, the dimensionless parameter β^* has been redefined to $\beta^* = 10^{-3}(1-y/3)^2$.

-
- [1] J. Keener and J. Sneyd, *Mathematical Physiology* (Springer-Verlag, New York, 1998).
- [2] B. Alberts *et al.*, *Molecular Biology of the Cell* (Garland, New York, 2002).
- [3] R. Cooke, *Physiol. Rev.* **77**, 671 (1997).
- [4] T. J. Burkholder and R. L. Lieber, *J. Exp. Biol.* **204**, 1529 (2001).
- [5] O. Farago and A. Bernheim-Groswasser, *Soft Matter* **7**, 3066 (2011).
- [6] A. V. Hill, *Proc. R. Soc. London, Ser. B* **126**, 136 (1938).
- [7] R. V. Mastrigt, *IEEE Trans. Biomed. Eng.* **27**, 413 (1980).
- [8] A. F. Huxley, *Prog. Biophys. Biophys. Chem.* **7**, 255 (1957).
- [9] H. E. Huxley, *J. Mol. Biol.* **7**, 281 (1963).
- [10] J. Kendrick-Jones, W. Lehman, and A. G. Szent-Gyorgyi, *J. Mol. Biol.* **54**, 313 (1970).
- [11] R. W. Lymn and E. W. Taylor, *Biochemistry* **10**, 4617 (1971).
- [12] T. A. J. Duke, *Proc. Natl. Acad. Sci. (USA)* **96**, 2770 (1999).
- [13] G. Lan and S. X. Sun, *Biophys. J.* **88**, 4107 (2005).
- [14] K. Kitamura, M. Tokunaga, S. Esaki, A. H. Iwane, and T. Yanagida, *Biophysics* **1**, 1 (2005).
- [15] S. Walcott and S. X. Sun, *Phys. Chem. Chem. Phys.* **11**, 4871 (2009).
- [16] A. Mansson, *Biophys. J.* **98**, 1237 (2010).
- [17] L. Marcucci and L. Truskinovsky, *Eur. Phys. J. E* **32**, 411 (2010).
- [18] B. Chen and H. Gao, *Biophys. J.* **101**, 396 (2011).
- [19] C. R. Worthington, *Nature (London)* **193**, 1283 (1962).
- [20] A. Landesberg and S. Sideman, *Am. J. Physiol.* **278**, H1274 (2000).
- [21] G. Piazzesi *et al.*, *Cell* **131**, 784 (2007).
- [22] M. Badoual, F. Jülicher, and J. Prost, *Proc. Natl. Acad. Sci. (USA)* **99**, 6696 (2002).
- [23] F. Jülicher and J. Prost, *Phys. Rev. Lett.* **78**, 4510 (1997).
- [24] M. J. I. Müller, S. Klumpp, and R. Lipowsky, *Proc. Natl. Acad. Sci. (USA)* **105**, 4609 (2008).
- [25] D. Hexner and Y. Kafri, *Phys. Biol.* **6**, 036016 (2009).
- [26] B. Gilboa, D. Gillo, O. Farago, and A. Bernheim-Groswasser, *Soft Matter* **5**, 2223 (2009).
- [27] P. Y. Placais, M. Balland, T. Guérin, J. F. Joanny, and P. Martin, *Phys. Rev. Lett.* **103**, 158102 (2009).
- [28] On the microscopic time scales of the power stroke, the velocity of the motor head changes and the motor force fluctuates between positive and negative values. In contrast, Hill’s equation applies to a coarse-grained picture where the thick and thin filaments are

treated as two objects sliding at relative velocity v . Therefore, the motor force expressed in Eq. (5) should be considered as an effective force that each attached motor generates between these two objects.

- [29] Y. C. Fung, *Biomechanics: Mechanical Properties of Living Tissues* (Springer-Verlag, New York, 1993).
- [30] N. Dharan and O. Farago, *Phys. Rev. E* **85**, 021904 (2012).
- [31] M. Linari, M. Caremani, and V. A. Lombardi, *Proc. R. Soc. B* **277**, 19 (2010).
- [32] C. Veigel and C. F. Schmidt, *Nat. Rev. Mol. Cell Biol.* **12**, 163 (2011).